Electrospun Nanofiber-Based Anodes, Cathodes, and Separators for Advanced Lithium-Ion Batteries

Article *in* Polymer Reviews · July 2011

DOI: 10.1080/15583724.2011.593390

CITATIONS
67

READS
2,506

5 authors, including:

Xiangwu Zhang
North Carolina State University
188 PUBLICATIONS **7,166** CITATIONS
SEE PROFILE

Liwen Ji
Enevate Corp.
56 PUBLICATIONS **5,882** CITATIONS
SEE PROFILE

Ozan Toprakçı
North Carolina State University
30 PUBLICATIONS **1,339** CITATIONS
SEE PROFILE

Mataz Alcoutlabi
University of Texas Rio Grande Valley
58 PUBLICATIONS **3,175** CITATIONS
SEE PROFILE

Polymer Reviews
Publication details, including instructions for authors and subscription information:
http://www.tandfonline.com/loi/lmsc20

Electrospun Nanofiber-Based Anodes, Cathodes, and Separators for Advanced Lithium-Ion Batteries

Xiangwu Zhang [a], Liwen Ji [a], Ozan Toprakci [a], Yinzheng Liang [a] & Mataz Alcoutlabi [a]

[a] Fiber and Polymer Science Program, Department of Textile Engineering, Chemistry and Science, North Carolina State University, Raleigh, North Carolina, 27695-8301, USA

Published online: 11 Aug 2011.

To cite this article: Xiangwu Zhang, Liwen Ji, Ozan Toprakci, Yinzheng Liang & Mataz Alcoutlabi (2011) Electrospun Nanofiber-Based Anodes, Cathodes, and Separators for Advanced Lithium-Ion Batteries, Polymer Reviews, 51:3, 239-264, DOI: 10.1080/15583724.2011.593390

To link to this article: http://dx.doi.org/10.1080/15583724.2011.593390

Polymer Reviews, 51:239–264, 2011

ISSN: 1558-3724 print / 1558-3716 online
DOI: 10.1080/15583724.2011.593390

Taylor & Francis
Taylor & Francis Group

Reviews

Electrospun Nanofiber-Based Anodes, Cathodes, and Separators for Advanced Lithium-Ion Batteries

XIANGWU ZHANG, LIWEN JI, OZAN TOPRAKCI, YINZHENG LIANG, AND MATAZ ALCOUTLABI

Fiber and Polymer Science Program, Department of Textile Engineering, Chemistry and Science, North Carolina State University, Raleigh, North Carolina 27695-8301, USA

Novel nanofiber technologies present the opportunity to design new materials for advanced rechargeable lithium-ion batteries. Among the various existing energy storage technologies, rechargeable lithium-ion batteries are considered as effective solution to the increasing need for high-energy electrochemical power sources. This review addresses using electrospinning technology to develop novel composite nanofibers which can be used as anodes, cathodes, and separators for lithium-ion batteries. The discussion focuses on the preparation, structure, and performance of silicon/carbon (Si/C) nanofiber anodes, lithium iron phosphate/carbon ($LiFePO_4$/C) nanofiber cathodes, and lithium lanthanum titanate oxide/polyacrylonitrile (LLTO/PAN) nanofiber separators. Si/C nanofiber anodes have the advantages of both carbon (long cycle life) and Si (high lithium-storage capacity). $LiFePO_4$/C nanofiber cathodes show good electrochemical performance including satisfactory capacity and good cycling stability. LLTO/PAN nanofiber separators have large electrolyte uptake, high ionic conductivity, and low interfacial resistance with lithium, which increase the capacity and improve the cycling stability of lithium-ion cells. These results demonstrate that electrospinning is a promising approach to prepare high-performance nanofiber anodes, nanofiber cathodes, and nanofiber separators that can potentially replace currently-used lithium-ion battery materials.

1. Introduction and Background

Today's world economy is dangerously dependent on fossil fuel, and this problem is exacerbated because heavily populated developing countries are expanding their economies and becoming more energy intensive. World energy demand is expected to double by the year 2050 and triple by the end of the century. In addition, air quality and global climate impact are other major concerns with the continuing dependence on dwindling fossil fuel sources. Therefore, there has been substantial interest in renewable energy sources such

Received April 17, 2011; accepted May 23, 2011.
Address correspondence to Xiangwu Zhang, Fiber and Polymer Science Program, Department of Textile Engineering, Chemistry and Science, North Carolina State University, Raleigh, North Carolina 27695-8301, USA. E-mail: xiangwu_zhang@ncsu.edu

as wind and solar. However, these technologies have a random and variable energy output which makes them difficult to manage. It is clear that the advancement of energy storage technologies is required for the effective utilization of renewable energy sources in future smart grids and power delivery systems.[1]

Among the various existing energy storage technologies, rechargeable lithium-ion batteries are considered as effective solution to the increasing need for high-energy electrochemical power sources. Rechargeable lithium-ion batteries offer energy densities 2–3 times and power densities 5–6 times higher than conventional Ni-Cd and Ni-MH batteries, and as a result, they weigh less, take less space, and deliver more energy.[2–4] In addition to high energy and power densities, lithium-ion batteries also have other advantages, such as high coulombic efficiency, low self-discharge, high operating voltage, and no "memory effect."[5]

Each lithium-ion battery consists of an anode and a cathode separated by an electrolyte containing dissociated lithium salts, which enables the transfer of lithium ions between the two electrodes, as illustrated in Fig. 1. The electrolyte is typically contained in a porous separator membrane that prevents the physical contact between the anode and cathode. When the battery is being charged, an external electrical power source injects electrons into the anode. At the same time, the cathode gives up some of its lithium ions, which move through the electrolyte to the anode and remain there. During this process, electricity is stored in the battery in the form of chemical energy. When the battery is discharging, the lithium ions move back across the electrolyte to the cathode, enabling the release of electrons to the outer circuit to do the electrical work. Current lithium-ion batteries were developed mainly for portable applications (such as cell phones and lap-tops) and they depend on using active powder materials (such as graphite powder in the anode and $LiFePO_4$ powder in the cathode) to store energy. However, powder materials have a long diffusion path for lithium ions and slow electrode reaction kinetics, and as a result, the performance of current lithium-ion batteries has not reached their potential.[6] Therefore, new energy-storage materials and electrodes must be developed to obtain advanced lithium-ion batteries that outperform current technologies and can be used in large-scale systems.

Electrospun nanofibers are attractive as electrode materials since they have a shorter diffusion path relative to the commonly employed powder materials and faster intercalation kinetics is expected due to their high area/mass ratio. Electrospun nanofibers also offer a

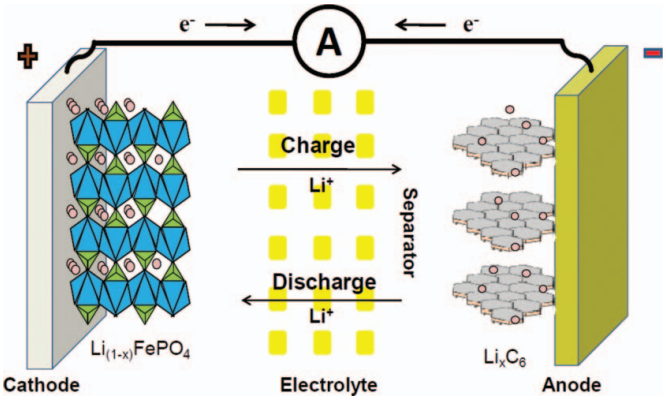

Figure 1. Schematic of a lithium-ion battery. Each lithium-ion battery consists of an anode and a cathode separated by an electrolyte containing dissociated lithium salts, which enables transfer of lithium ions between the two electrodes (Color figure available online).

relatively large number of lithium insertion sites, and therefore the charge-transfer resistance at the interface between the electrolyte and active electrode materials is decreased. Hence, electrospun nanofibers are advantageous for use as electrode materials in lithium-ion battery applications.

In addition to electrodes, the separator plays an important role by regulating cell kinetics, preventing electronic contact between electrodes, and maintaining liquid electrolyte in cells.[7–10] At present most lithium-ion batteries use conventional microporous polyolefin membranes as the separator. Polyolefin microporous membranes have good chemical stability, suitable thickness, and reasonable mechanical strength, but they have low thermal stability, low porosity, and poor wettability with polar liquid electrolyte, which lead to high cell resistance, reduced energy density, and low rate capability of rechargeable lithium-ion batteries.[7–12] Recently, it was found that electrospun nanofiber mats have small pore size and large porosity, and can be directly used as separators in rechargeable lithium-ion batteries.[10–15] Electrospun nanofiber separators enable high-rate charge/discharge of batteries because of their high porosity and desirable pathways for ion transport.

Recent work from our laboratory has focused on developing novel electrospun nanofibers for lithium-ion battery applications. Results demonstrate that lithium-ion batteries using electrospun nanofiber anodes, cathodes, and separators have excellent overall performance including large capacity, high charge/discharge rate capability, and extended cycle life. In this article, we first give a brief review on the electrospinning of nanofibers of different materials, including polymers, carbons, and ceramics. Then, we review our recent developments on novel silicon/carbon (Si/C) nanofiber anodes, lithium iron phosphate/carbon ($LiFePO_4$/C) nanofiber cathodes, and lithium lanthanum titanate oxide/polyacrylonitrile (LLTO/PAN) nanofiber separators using the electrospinning process.

2. Electrospinning of Nanofibers

Electrospinning is a simple, non-mechanical technique that has gained attention due to its capability and feasibility to generate large quantities of nanofibers with well-defined topologies at relatively low cost.[16–18] Figure 2 shows a schematic diagram of the basic setup for electrospinning. A high voltage is applied between a polymer solution contained in a syringe and a metallic collector. This causes the polymer solution to elongate forming a "Taylor cone" at the needle tip. When the voltage reaches a critical value, electrostatic forces overcome the surface tension of the polymer solution and eject a liquid jet from

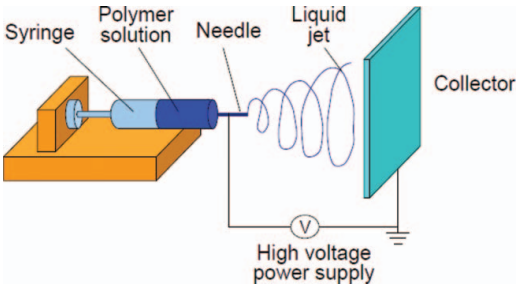

Figure 2. Schematic of an electrospinning setup. The electrically-charged jet undergoes a stretching-and-whipping process, which is accompanied by the rapid evaporation of the solvent to reduce the jet diameter from hundreds of micrometers to as small as tens of nanometers (Color figure available online).

the nozzle of the spinneret (metallic needle). The electrically-charged jet then undergoes a stretching-and-whipping process resulting in the formation of a long, thin thread. This stretching-and-whipping process is accompanied by the rapid evaporation of the solvent that reduces the jet diameter from hundreds of micrometers to as small as tens of nanometers. Dry fibers are accumulated on the surface of the collector forming a nonwoven mat of polymer nanofibers. The process can be adjusted to control the fiber diameter by varying the applied voltage and polymer solution concentration (or viscosity). The duration of the electrospinning procedure controls the thickness of the fiber deposition.[19] Through careful control of processing parameters, electrospun nanofiber mats can also be produced over a wide range of porosity values.[20]

Although most current electrospinning research focuses on the fabrication of polymer nanofibers, carbon nanofibers can also be prepared by carbonization of fibers electrospun from different types of precursor polymers, such as polyacrylonitrile (PAN), polyimide (PI), and pitch.[21–24] The carbonization temperature can be adjusted to control the carbon crystalline structure and, hence, the mechanical and functional properties of carbon nanofibers.[21–23] In addition to carbon nanofibers, ceramic nanofibers can be synthesized by electrospinning their precursor solutions, followed by calcination. Ceramic nanofibers synthesized by electrospinning were reported first in 2002;[25,26] since then, more than twenty ceramic systems (e.g., SiO_2, Al_2O_3, and ZrO_2)[16,27–35] have been fabricated as nanofibers.[25,26] These fibers can be amorphous, polycrystalline, dense, porous, or hollow.[26]

Traditionally, electrospinning was considered a slow process. It often takes hours for a set-up shown in Fig. 2 to generate a free-standing nanofiber mat. However, the industry has developed and commercialized large-scale electrospinning machines for mass production of nanofibers. Companies that produce large-scale electrospinning machines include but are not limited to Elmarco, ANSTCO, MECC, Fuence, and Yflow. The production rates of these machines are sufficient for many practical applications. Compared with most nanotechnologies, electrospinning is a relatively low-cost process; hence, it has been used for manufacturing commercial products by many companies, such as Freudenberg Nonwovens, Donaldson Company, and eSpin Technologies.

3. Nanofiber Anodes

Significant efforts have been made to use electrospinning to develop advanced nanofiber anodes for lithium-ion batteries. Table 1 shows examples of nanofiber anodes developed recently.[36–51] To obtain high-performance nanofiber anodes, it is important to selectively appropriate active materials to make nanofibers. Carbon (such as graphite) is presently the most utilized anode material for lithium-ion batteries due to its low and flat working potential, long cycle life, and low cost. However, the most lithium-enriched intercalation compound of graphite only has a stoichiometry of LiC_6, resulting in less-than-desirable theoretical charge capacity (370 mAh g^{-1}).[38,52] To improve the anode capacity, non-carbon materials, which can incorporate large amounts of lithium, have been developed. Among various non-carbon materials, Si is found to have the highest theoretical capacity of 4200 mAh g^{-1}.[52] However, the high capacity of Si leads to large volume change of the anode since a significantly higher amount of lithium is inserted and de-inserted during cycling. As a result, the major problem associated with the use of Si is the mechanical failure of this brittle material brought about by large-volume change during lithium insertion/extraction. Many approaches have been used to reduce the large volume change during the lithium insertion/de-insertion and therefore to obtain better capacity retention and cycle life for Si anodes.[52] Here, we discuss the approach to solve the poor mechanical stability of

Table 1
Materials, precursors, electrospinning conditions, and main features of various electrospun nanofiber anodes

Materials	Precursors	Electrospinning conditions	Main features	References
Si/C	Si, PAN	17 kV, 15 cm, 0.75 mL h^{-1}	Short lithium ion diffusion distance, large reversible capacity, and relatively good cycling performance	37
Si/C	Si, PAN	21 kV, 15 cm, 0.75 mL h^{-1}	High Si content, short lithium ion diffusion distance, and large reversible capacity	38
Si/C	Si, PAN PLLA	21 kV, 15 cm, 0.75 mL h^{-1}	Porous carbon matrix, high surface area, large reversible capacity, and relatively good cycling performance	36
Si/C	Si, PVA	20 kV, 11 cm, 1 mL h^{-1}	Controllable size and surface area, and graduate increase in capacity	39
Ni/C	$[Ni(OAc)_2]\cdot 4H_2O$, PAN	12.5 kV, 15 cm, 0.5 mL h^{-1}	High electronic conductivity, high rate capacity	40
Cu/C	$Cu(CH_3COO)_2$, PAN	10.5 kV, 15 cm, 0.5 mL h^{-1}	High electronic conductivity, facile electronic/ionic transfer, and high rate capacity	41
Co/C	$Co(CH_3COO)_2\cdot 4H_2O$, PAN	10-11 kV, 12 cm, 2.5 μL min^{-1}	Reduced Li-ion diffusion distance	43
Sn/C	Tin octoate, PAN, PMMA	15 kV, 16 μL min^{-1}	Porous multichannel carbon tubular shell, and high Sn parking density	44
Sn/C	Tributyltin, PAN, mineral oil	20 kV, 15 cm, 15 (outer) and 5 (inner) μL min^{-1}	Hollow carbon nanofibers, and high electrode-electrolyte contact	45
Sn/C	$SnCl_2\cdot H_2O$, PVA,	25 kV, 15 cm, 1 mL h^{-1}	Small Sn particle size (1 nm), Sn partially oxidized during preparation, and oxidized Sn reduced during cycling	46

(Continued on next page)

Table 1
Materials, precursors, electrospinning conditions, and main features of various electrospun nanofiber anodes *(Continued)*

Materials	Precursors	Electrospinning conditions	Main features	References
MnO_x/C	$Mn(CH_3COO)_2$, PAN	14 and 21 kV, 15 cm, 0.75 mL h^{-1}	Porous carbon nanofibers, large surface area, good mechanical stability, and high conductivity	47,48
Fe_3O_4/C	$Fe(C_5H_7O_2)_3$, PAN	12-14 kV, 12 cm, 4 μL min^{-1}	Large volume changed digested during conversion reaction, and high reversible capacity	42
Porous C	SiO_2, PAN	21 kV, 15 cm, 0.8 mL h^{-1}	Highly develop pore structure, large surface area and porosity, and enhance charge-discharge kinetics	49
Porous C	$ZnCl_2$, PAN	14 kV, 15 cm, 0.5 mL h^{-1}	Activated carbon, huge surface area, small pore size, increased capacity, and enhanced cycling performance	50
Porous C	PLLA, PAN	17 kV, 15 cm, 0.5 mL h^{-1}	Large surface area, small pore size, stable cycling performance	51

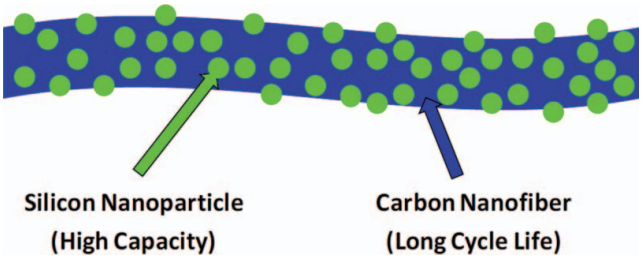

Figure 3. Schematic of a Si/C nanofiber. The carbon matrix can accommodate the large volume change of Si nanoparticles during charge/discharge (Color figure available online).

Si by incorporating nano-scale Si particles into carbon nanofibers (Fig. 3) through the carbonization of electrospun Si/PAN nanofibers. In the resultant Si/C nanofibers, the carbon matrix can accommodate the large volume change of Si during charge/discharge.

3.1 Preparation of Nanofiber Anodes

Un-oxidized Si nanoparticles with sizes ranging from 30 and 50 nm were dispersed in PAN solutions in dimethylformamide (DMF) by mechanically stirring. A variable high-voltage power supply (Gamma ES40P-20W/DAM) was used to provide a high voltage (around 21 kV) for electrospinning. The flow rate used was 0.75 mL h^{-1} and the needle-to-collector distance was 15 cm. Electrospun Si/PAN composite nanofibers were stabilized in air environment at 280°C for 5 hours (the heating rate was 5°C/min) and then carbonized at 700°C for 1 hour in a nitrogen atmosphere (the heating rate was 2°C min^{-1}) to form Si/C nanofibers. For more details on the preparation of these Si/C nanofibers, the reader is referred to references.[49,53,54]

3.2 Structure of Nanofiber Anodes

Figure 4 illustrates scanning electron microscopy (SEM) images of electrospun 15 wt% Si/PAN nanofibers. It is seen that the distribution of Si nanoparticles in the PAN matrix is relatively homogeneous. SEM images of Si/C nanofibers prepared from 15 wt% Si/PAN precursor are illustrated in Fig. 5. Compared with the corresponding Si/PAN precursor nanofibers shown in Fig. 4, Si/C nanofibers are less straight and more Si nanoparticles are exposed on the fiber surface.

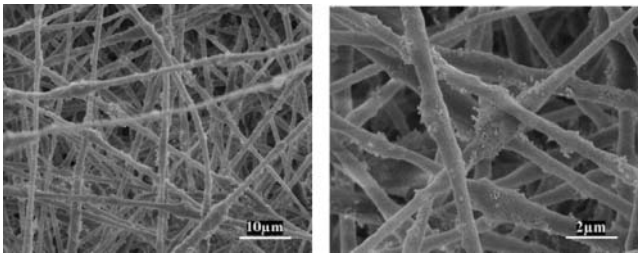

Figure 4. SEM images of electrospun 15 wt% Si/PAN nanofibers with different magnifications. Si nanoparticles are distributed in the PAN matrix.

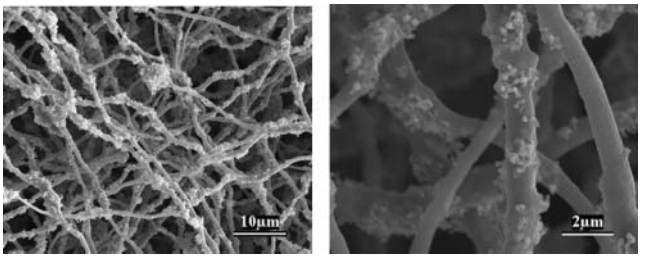

Figure 5. SEM images of Si/C nanofibers prepared from 15 wt% Si/PAN precursor. Compared with Si/PAN precursor nanofibers shown in Fig. 4, Si/C nanofibers are less straight and more Si nanoparticles are exposed on the fiber surface.

X-ray diffraction (XRD) pattern of Si/C nanofibers is shown in Fig. 6. For comparison, XRD pattern of pure carbon nanofibers is also shown. It is seen that pure carbon nanofibers exhibit a diffraction peak at $2\theta = 25.0^{o}$, which is corresponding to the (002) layers of the graphite.[55–57] However, that peak is weak and broad, indicating that the nanofibers are largely formed by disordered carbon. Si/C composite nanofibers present diffraction peaks at 2θ of around 28.4°, 47.4°, 56.2°, 69.2°, 76.5°, and 88.1°, which are ascribed to the (111), (220), (311), (400), (331), and (422) planes of Si crystals in nanofibers, respectively.[55,58–62] From SEM images and XRD patterns, it can be concluded that Si/C nanofibers have been successfully prepared using electrospinning combined with heat treatment.

3.3 Electrochemical Performance of Nanofiber Abodes

Electrospun Si/C nanofibers form free-standing, flexible nonwoven mats. They were directly used as the lithium-ion battery anode without introducing any post-treatment step. The electrochemical performance of Si/C nanofiber anodes was investigated by carrying out galvanostatic charge-discharge tests at a constant current density of 50 mA g^{-1}. Figures 7 and 8 show the charge-discharge curves of pure Si and Si/C nanofiber anodes, respectively. The Si anode was prepared by mixing 80 wt% of Si nanoparticles with 10 wt% of

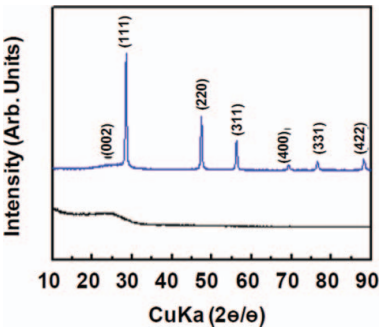

Figure 6. XRD patterns of carbon and Si/C nanofibers prepared from PAN and 15 wt% Si/PAN precursors. Si/C composite nanofibers present diffraction peaks at 2θ of around 28.4°, 47.4°, 56.2°, 69.2°, 76.5°, and 88.1°, which are ascribed to the (111), (220), (311), (400), (331), and (422) planes of Si crystals in nanofibers, respectively. The broad diffraction peak at $2\theta = 25.0^{o}$ (002) indicates the carbon matrix has a disordered structure (Color figure available online).

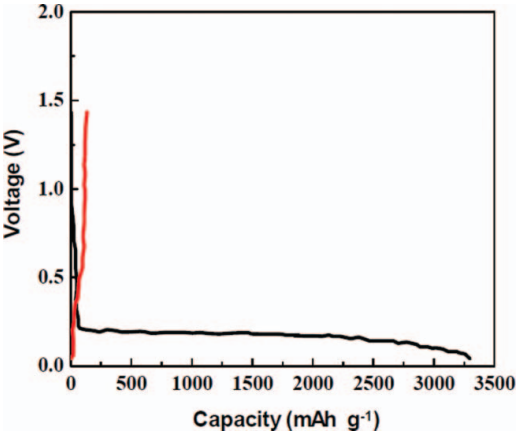

Figure 7. Charge-discharge curves of Si anode. A charge capacity of up to 3300 mAh g^{-1} is achieved during lithium insertion. However, during lithium extraction, the discharge capacity of Si anode is only 113 mAh g^{-1} due to the large volume change of Si. (Color figure available online).

polyvinylidene fluoride binder and 10 wt% of carbon black conductor.[38] It can be seen in Fig. 7 that during lithium insertion a potential plateau appears approximately at 0.2 V with a charge capacity up to 3300 mAh g^{-1}. However, the high Li packing density results in a large volume change during the insertion process, which results in anode cracking and therefore a total loss of the capacity. As a result, during lithium extraction, the actual capacity of Si anode is only 113 mAh g^{-1}, which is even much lower than that of graphite. However, Si/C nanofiber anode shows good re-chargeability. As shown in Fig. 8, at the first cycle, the Si/C nanofiber anode made from 15 wt% Si/PAN precursor has a specific charge capacity of approximately 1100 mAh g^{-1} and discharge capacity of 880 mAh g^{-1},

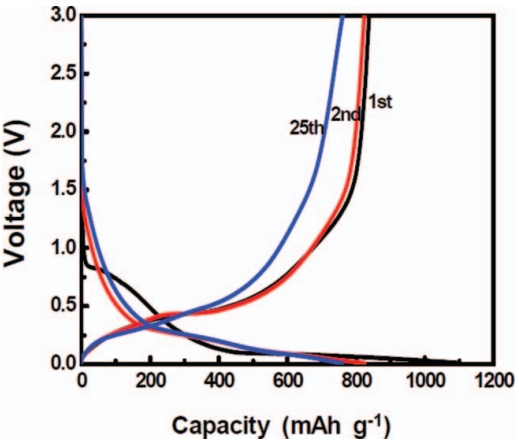

Figure 8. Charge-discharge curves of Si/C nanofiber anode prepared from 15 wt% Si/PAN precursor. At the first cycle, the Si/C nanofiber anode has a specific charge capacity of approximately 1100 mAh g^{-1} and discharge capacity of 880 mAh g^{-1}, which are significantly greater than the theoretical capacity (370 mAh g^{-1}) of graphite (Color figure available online).

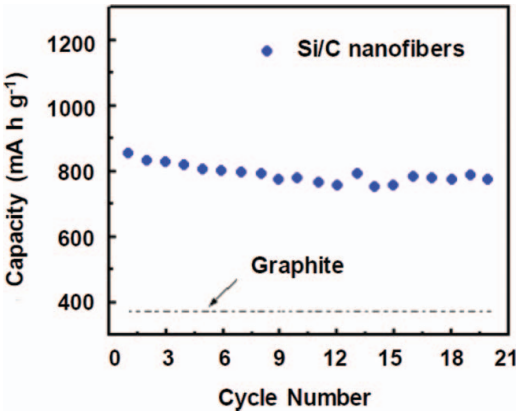

Figure 9. Cycling performance of Si/C nanofiber anode prepared from 15 wt% Si/PAN precursor. The capacity of Si/C nanofiber anode is greater than that of graphite and is relatively stable in at least the first 20 cycles (Color figure available online).

which are significantly greater than the theoretical capacity (370 mAh g^{-1}) of graphite. Therefore, the encapsulation of Si nanoparticles in the carbon matrix can accommodate the large volume change of Si during charge/discharge, and the resultant Si/C nanofibers have high capacities and are rechargeable.

Figure 9 shows the cycling performance of Si/C nanofibers. It is obvious that the electrochemical performance of the anode is improved by incorporating the Si into the carbon nanofibers. The capacity of Si/C nanofibers is significantly higher than the theoretical value of graphite. In addition, with an increase in the cycle number, the capacity of Si/C nanofibers remains relatively constant, indicating that these anode nanofibers have good cycling stability. It can hence be concluded that Si/C nanofibers combine the advantages of Si (high capacity) and carbon (long cycle life).

The concentration of Si nanoparticles in the Si/PAN precursor has significant effect on the electrochemical performance of the resultant Si/C nanofibers.[37,38] Typically, when the Si concentration is lower than 15wt%, the capacity of the Si/C nanofiber anode decreases since there are less high-capacity Si nanoparticles available. When the Si concentration is higher than 15wt%, the anode capacity increases; however, the cycling performance becomes poorer.

4. Nanofiber Cathodes

Similar to anodes, electrospinning can also be used to fabricate advanced nanofiber cathodes. Table 2 shows recent progress in preparing nanofiber cathodes using the electrospinning method.[63–69] Here we discuss the preparation, structure, and performance of $LiFePO_4$/C nanofiber cathodes. Among various alternative cathode materials, lithium iron phosphate ($LiFePO_4$), which was discovered by Goodenough in 1997,[70] is gaining significant attention because of its relatively low cost, high discharge potential (very flat voltage curve around 3.4 V versus Li/Li^+), large specific capacity (170 mAh g^{-1}), good thermal stability, excellent cycling performance, and high abundance with the environmentally benign and safe nature. However, $LiFePO_4$ has low conductivity ($\sim 10^{-9}$ S/cm), which leads to high impedance and low rate capability.[71] In our laboratory, electrospinning was used

Table 2
Materials, precursors, electrospinning conditions, and main features of various electrospun nanofiber cathodes

Materials	Precursors	Electrospinning conditions	Main features	References
$LiFePO_4$/C	$LiCOOCH_3$, H_3PO_4, $Fe(COOCH_3)_2$, PAN	15 kV, 15 cm	Thin carbon coating, and stable cycling performance	64
$LiCoO_2$	Lithium acetate, cobalt acetate, and citric acid	25 kV, 30 cm	Fast Li ion diffusion, and high first-cycle capacity	63
$LiCoO_2$	Lithium chloride, cobalt acetate, and PVA	12 kV	High surface area, and spinel structure	65
$LiCoO_2$	Li(OiPr), $Co(C_2H_3O_2)_2{\cdot}4H_2O$, PVP	1.2 kV, 2 cm	3-D architecture, layered structure, high rate capability, and good reversibility	67
$LiCoO_2$/MgO	Lithium acetate, cobalt acetate, magnesium acetate, and citric acid,	25 kV, 30 cm	Core ($LiCoO_2$)-shell (MgO) structure, excellent reversibility, and small impedance growth	66
$LiNi_{1/3}Co_{1/3}Mn_{1/3}O_2$	Lithium nitrate, Nickel nitrate, cobalt nitrate, manganese nitrate, PVP	25 kV, 15 cm	Layered structure, high surface area, and good capacity retention	68
$LiNi_{3/8}Co_{1/4}Mn_{3/8}O_2$	Lithium nitrate, Nickel nitrate, cobalt nitrate, manganese nitrate, PVP	25 kV, 15 cm	Layered structure, high surface area, and good capacity retention	68
Al doped $LiNi_{1/3}Co_{1/3}Mn_{1/3}O_2$	Lithium nitrate, Nickel nitrate, cobalt nitrate, manganese nitrate, aluminum nitrate, PVP	25 kV, 15 cm	Superior capacity, and good cycling performance	69

to obtain $LiFePO_4$/C nanofibers that have high conductivity and excellent electrochemical performance. Spinning solutions consisted of PAN and $LiFePO_4$ precursor. After electrospinning, PAN was converted into carbon through a heat treatment step, during which $LiFePO_4$ precursor transformed to active $LiFePO_4$. Hence, PAN was not only used as an electrospinning media for providing the spinnability of precursor solutions but also as a carbon source in order to increase the conductivity of $LiFePO_4$. Unlike in most studies such as mixing or coating $LiFePO_4$ with a conducting material, here, conductive coating and $LiFePO_4$ formation take place together in one step, which ensures nano-scale carbon coating on the particle surface and maximizes the $LiFePO_4$-carbon interface.

4.1 Preparation of Nanofiber Cathodes

Carbon precursor, PAN, was first dissolved in DMF at room temperature by stirring for 24 h. For $LiFePO_4$ precursor, $LiCOOCH_3$, H_3PO_4, and $Fe(COOCH_3)_2$ were used as the starting materials and mixed in DMF at a stoichiometric ratio of 1:1:1 by stirring at room temperature for 24 h. Separately prepared PAN and $LiFePO_4$ precursor solutions were mixed to obtain electrospinning solutions. The electrospinning process was similar to that used in the preparation of Si/C nanofiber anodes. Electrospinning conditions used were: voltage = 15 kV, and needle-to-collector distance = 15 cm. Electrospun $LiFePO_4$ precursor/PAN nanofibers were heat treated in two steps. In the first step, nanofibers were stabilized under air. The process started at room temperature and reached 280°C with a heating rate of 5°C/min. That temperature was maintained for 5 h to complete the stabilization process, during which the cyano side groups of PAN form cyclic rings mainly by a dehydrogenation process.[72] In the second step, nanofibers were calcined (for $LiFePO_4$ formation) and carbonized (for carbon formation) simultaneously at 700°C for 18 h under argon atmosphere. During calcination/carbonization, $LiFePO_4$ precursor transformed to energy-storage $LiFePO_4$ material and PAN became electrically-conducting carbon.

4.2 Structure of Nanofiber Cathodes

Figure 10 shows the XRD pattern of $LiFePO_4$/C nanofibers. For comparison, the reference data[73] of pristine $LiFePO_4$ are also shown. It is seen that all diffraction peaks of $LiFePO_4$/C nanofibers are indexed to an olivine $LiFePO_4$ with orthorhombic crystal structure (Space Group: Pnma) and there are no impurity phase peaks. The average crystallite size was calculated to be 20 nm by using the full widths at half maximum (FWHM or β) of (2 0 0), (1 0 1), and (2 0 1) or (1 1 1), (0 2 0), and (3 1 1) peaks.

SEM analyses of electrospun $LiFePO_4$ precursor/PAN and heat-treated $LiFePO_4$/C nanofibers were carried out, and results are shown in Fig. 11. It is seen from Fig. 11a that a "network-like" structure is obtained by the electrospinning of the $LiFePO_4$ precursor/PAN solution. However, beads are formed and variations in the fiber diameter are also observed. The average fiber diameter of electrospun $LiFePO_4$ precursor/PAN nanofibers is around 125 nm. Heat treatment has influence on the morphology of electrospun nanofibers. From Fig. 11b, it is seen that after heat treatment, the nanofiber structure is still maintained; however, more beads are formed. Substantial fiber diameter decrease is also observed because of the removal of some species (such as CO_2, HCN, and NH_3, etc.) from the structure during heat treatment. The average diameter of nanofibers decreases from 125 to 90 nm after heat treatment.

The carbon content of heat-treated $LiFePO_4$/C nanofibers was measured using elemental analysis and it is 17.0 wt%. Figure 12 shows a SEM image of $LiFePO_4$/C nanofibers

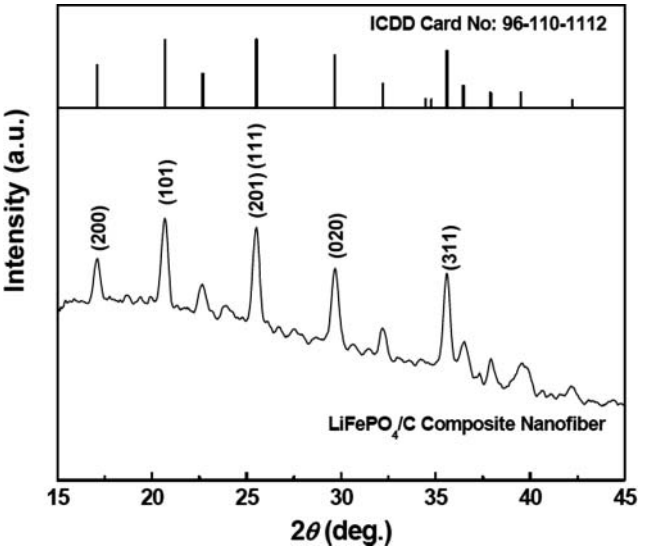

Figure 10. XRD pattern of $LiFePO_4$/C nanofibers and the reference XRD data of pristine $LiFePO_4$. All diffraction peaks of $LiFePO_4$/C nanofibers are indexed to an olivine $LiFePO_4$ with orthorhombic crystal structure (Space Group: Pnma) and there are no impurity phase peaks.

and its corresponding EDS maps of phosphorus, iron, carbon, and oxygen. Uniform element distribution of iron, phosphorus, and oxygen can be seen clearly. In addition to SEM and EDS analyses, further evaluation was carried out by transmission electron microscopy (TEM) in order to determine the particle microstructure and carbon coating characteristic. Figure 13 shows a TEM image of $LiFePO_4$/C nanofibers. It is seen that $LiFePO_4$ nanoparticles are embedded in carbon nanofibers. The resultant $LiFePO_4$/C nanofibers have a thin carbon coating of 8 nm.

4.3 Electrochemical Performance of Nanofiber Cathodes

Electrospun and heat-treated $LiFePO_4$/C nanofibers were directly used as the cathode in lithium-ion cells without any post-treatment. The first-cycle charge-discharge curves of the $LiFePO_4$/C nanofiber cathode are illustrated in Fig. 14. Flat voltage plateaus at discharge

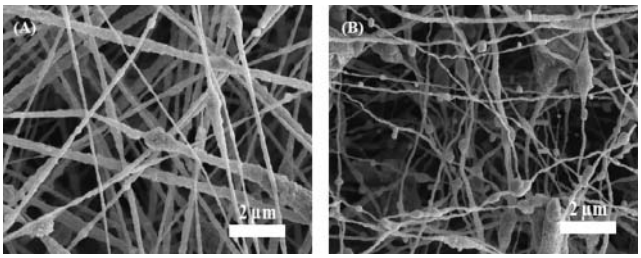

Figure 11. SEM images of (A) $LiFePO_4$ precursor/PAN nanofibers and (B) the resultant $LiFePO_4$/C nanofibers. After heat treatment, the nanofiber structure is still maintained; however, more beads are formed. Substantial fiber diameter decrease is also observed.

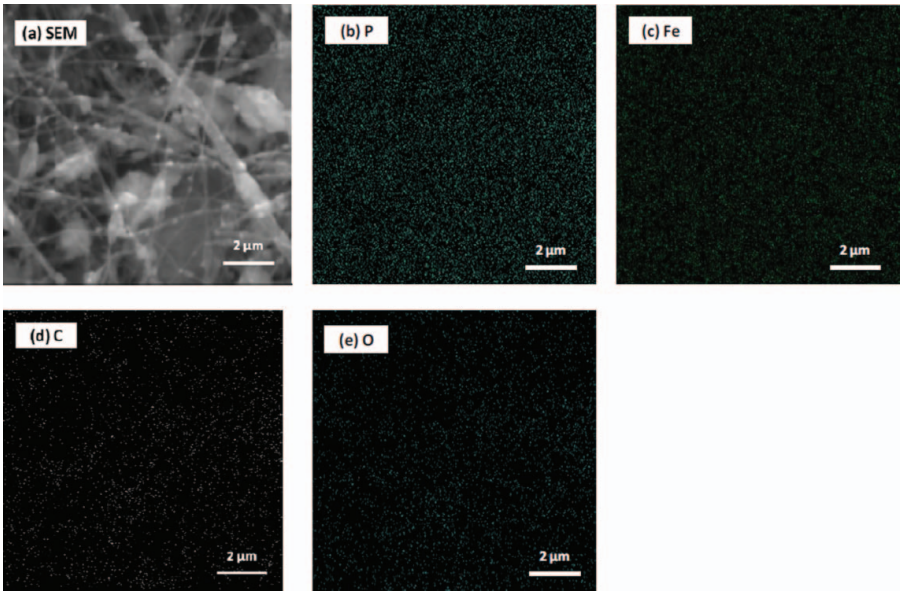

Figure 12. SEM image (a) and corresponding EDS maps of phosphorus (b), iron (c), carbon (d) and oxygen (e) in $LiFePO_4$/C nanofibers. Uniform element distribution of phosphorous, iron, and oxygen can be seen clearly (Color figure available online).

and charge can be observed around 3.35 and 3.55 V, respectively, which are the main characteristic of the two-phase reaction of $LiFePO_4$. It is also seen that both the charge and the discharge capacities of the $LiFePO_4$/C nanofiber cathode are greater than 140 mAh g^{-1} at the first cycle. Figure 15 shows the cycling performances of $LiFePO_4$/C nanofiber cathode. It is seen that no apparent capacity loss is observed during cycling.

Figure 16 shows the rate capability of these $LiFePO_4$/C nanofibers. Average discharge capacities are obtained as 162, 153, 136, 98, 71, and 37 mAh g^{-1} at C/20, C/10, C/5, C/2, 1C, and 2C, respectively. Although the rate capability results are relatively good, they are still inadequate for certain applications, such as electrical vehicles or hybrid electrical vehicles. To overcome this problem, work is being carried out to increase the electronic and ionic

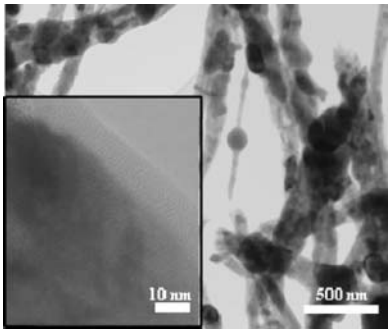

Figure 13. TEM image of $LiFePO_4$/C nanofibers. $LiFePO_4$ nanoparticles are embedded in carbon nanofibers, and the resultant $LiFePO_4$/C nanofibers have a thin carbon coating of 8 nm.

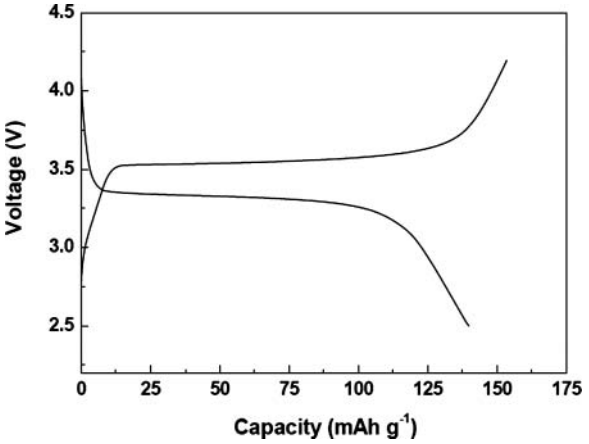

Figure 14. Charge-discharge curves of $LiFePO_4$/C nanofiber cathode. Flat voltage plateaus can be observed between 3.31–3.54 V and 3.26–3.55 V, which are the main characteristic of the two-phase reaction of $LiFePO_4$. Both charge and discharge capacities of the $LiFePO_4$/C nanofiber cathode are greater than 140 mAh g^{-1} at the first cycle.

conductivities of the composite nanofibers. Work is also being conducted on establishing the processing-structure-performance relationships for these novel composite nanofibers and the use of such fundamental knowledge to achieve high-performance $LiFePO_4$/C nanofibers that can be used in the next-generation lithium-ion batteries.

5. Nanofiber Separators

Separator is a porous membrane placed between the anode and cathode of a battery. Its main function is to prevent physical contact of the electrodes while serving as the electrolyte reservoir to enable ionic transport. Currently, most lithium-ion batteries use conventional microporous polymer membranes as the separator. Microporous polymer membranes have

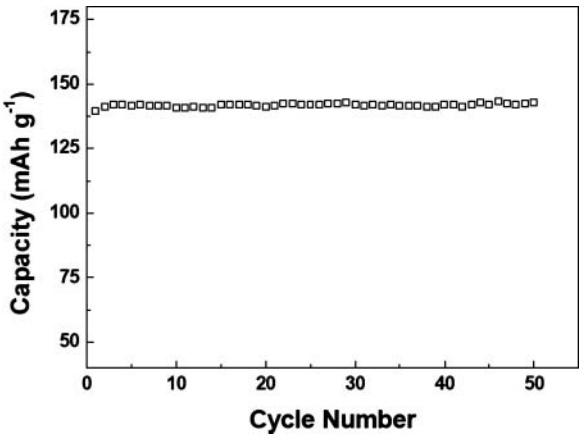

Figure 15. Cycling performance of $LiFePO_4$/C nanofiber cathode. No apparent capacity loss is observed during cycling.

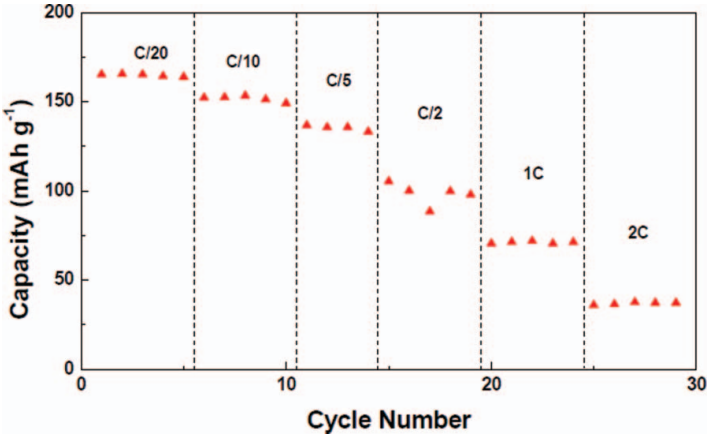

Figure 16. Rate capability of $LiFePO_4$/C nanofiber cathode. Average discharge capacities are obtained as 162, 153, 136, 98, 71, and 37 mAh g^{-1} at C/20, C/10, C/5, C/2, 1C, and 2C, respectively (Color figure available online).

good chemical stability, suitable thickness, and reasonable mechanical strength, but they have low thermal stability, low porosity, and poor wettability with polar liquid electrolyte, which in turn lead to high cell resistance, reduced energy density, and low rate capability of rechargeable lithium-ion batteries.[7–12] Recently, electrospinning technology has been used to fabricate novel nanofiber-based nonwoven membranes, which have a small pore size and large porosity, and can be directly used as separators in rechargeable lithium-ion batteries.[10–15] Table 3 shows the materials, electrospinning conditions, and main features of nanofiber separators developed recently.[13,74–77] These electrospun nanofiber separators enable high-rate charge/discharge of lithium-ion batteries because of their high porosity and desirable pathways for ion transport.

In our laboratory, ionic-conducting ceramic particles were introduced into electrospun PAN nanofibers to provide the opportunity to obtain porous nonwoven membranes that not only have the basic functions of battery separators, but also can conduct lithium ions, which can significantly improve the battery kinetics. Perovskite-type lithium lanthanum titanate, $Li_{3x}La_{2/3-x}TiO_3$ (abbreviated as LLTO), was used as the ionic-conducting ceramic due to its high bulk lithium-ion conductivity of about 10^{-3} S/cm at room temperature.[78] Our results show that the introduction of LLTO particles into electrospun nanofibers can combine the advantageous properties of both components and lead to new composite separators that have large liquid electrolyte uptake, high ionic conductivity, good electrochemical stability, improved safety, and reduced electrode-electrolyte interface resistance. As a result, the new LLTO/PAN nanofiber separators can provide desirable structure and properties for separating electrodes, supporting electrolytes, and transferring lithium ions, and lithium-ion batteries using these nanofiber separators can achieve good battery performance, such as large capacity, good cycleability, high rate capability, and enhanced safety.

5.1 Preparation of Nanofiber Separators

Lithium-ion conducting LLTO particles were prepared by the sol-gel method starting from stoichiometry amount (0.35:0.55:1.00) of $LiNO_3$, $La(NO_3)_3{\cdot}6H_2O$, and $Ti(OC_4H_9)_4$.[15–21]

Table 3
Materials, precursors, electrospinning conditions, and main features of various electrospun nanofiber separators

Materials	Precursors	Electrospinning conditions	Main features	References
PVDF	PVDF	8-15 kV, 0.1 mL min^{-1}	Good physical properties, good cycling capability, and small capacity loss	74
P(VDF-HFP)	P(VDF-HFP)	—	Good electrochemical stability, high capacity, and improved cycling performance	77
PAN	PAN	14 kV, 8 cm, 1.2 mL h^{-1}	Superior rate-capabilities, good cycling performance, and smaller diffusion resistance	76
SiO_2/PAN	SiO_2, PAN	20 kV, 17 cm, 1 mL h^{-1}	Large electrolyte uptake, and stable cycling performance	13
$Li_{3x}La_{2/3-x}TiO_3$/PAN	$LiNO_3$, $La(NO_3)_3{\cdot}6H_2O$, and $Ti(OC_4H_9)_4$, and PAN	18 kV, 18 cm, 0.5 mL h^{-1}	Great liquid electrolyte uptake, high electrochemical stability window, and low interfacial resistance with lithium	75

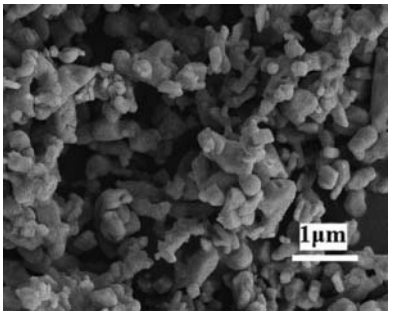

Figure 17. SEM image of LLTO particles. The size of the particles ranges from tens of nm to hundreds of nm, with an average size of 200 nm.

The aqueous precursor solution was kept at 80°C for 30 min with magnetic stirring to get a homogeneous gel, followed by drying at 150°C. The dried mixture was pyrolyzed at 350°C for 4 h and then calcined at 900°C for 2 h with the heating rate of 5°C/min. The calcined product was ground in an agate mortar and then sieved through a #325 mesh.

LLTO/PAN nanofiber separators were prepared by electrospinning DMF solutions of 8 wt% PAN containing different amount of LLTO particles (0, 5, 10, and 15 wt%), which were prepared at 70°C with mechanical stirring for at least 24 h. Electrospinning conductions used were: voltage = 18 kV, flow rate = 0.5 mL/hr, and needle-to-collector distance = 18 cm. Electrospun nanofibers were accumulated on the aluminum foil placed on the grounded collector to form porous nonwoven membranes. The resultant nanofiber-based porous membranes were dried in vacuum at 60°C for 12 h. For more details on the preparation of LLTO/PAN nanofiber separators, the reader is referred to reference number 75.

5.2 Structure of Nanofiber Separators

Figure 17 shows the SEM image of LLTO particles. It is seen that the size of the particles ranges from tens of nm to hundreds of nm, with an average size of 200 nm. Figure 18 shows SEM images of LLTO/PAN nanofibers with different LLTO contents. Pure PAN nanofibers (0 wt% LLTO) have a smooth surface, and are relatively uniform, taut and randomly oriented, forming a spider web-like interwoven network. The average diameter of these nanofibers is about 250 nm. The addition of 5 wt% LLTO leads to the formation of a small number of irregularities and uneven surface morphology, and the resultant LLTO/PAN nanofibers display an average diameter of about 230 nm. With further increase in LLTO content (e.g., 10 and 15 wt%), the surface roughness of the electrospun LLTO/PAN nanofibers increases, and some LLTO particles begin to agglomerate and form clusters. In addition, the average diameters of these nanofibers become smaller than 200 nm.

5.3 Electrochemical Performance of Nanofiber Separators

Electrospun LLTO/PAN nanofibers form free-standing, durable, and porous membranes that were directly used as separators in batteries without any post-treatment. Figure 19 shows the liquid electrolyte uptakes as a function of LLTO content for LLTO/PAN nanofiber separators at room temperature. The liquid electrolyte used was 1 M lithium hexafluorophosphate ($LiPF_6$) in 1:1 (V/V) ethylene carbonate/ethyl methyl carbonate. It is seen

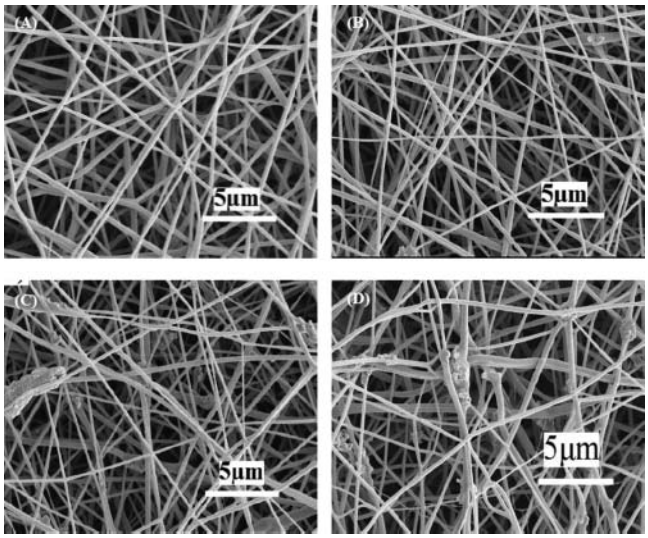

Figure 18. SEM images of LLTO/PAN nanofibers with different LLTO contents: (A) 0, (B) 5, (C) 10, and (D) 15 wt%. With increase in LLTO content, the surface roughness of the electrospun LLTO/PAN nanofibers increases, and some LLTO particles begin to agglomerate and form clusters.

that the electrolyte uptake increases slightly with increase in LLTO content. Figure 20 shows the temperature dependence of the ionic conductivities of liquid electrolyte-soaked LLTO/PAN nanofiber separators. It is seen that, for all four liquid electrolyte-soaked separators, the ionic conductivities increase with increase in temperature. In addition, the presence of LLTO particles has influence on the conductivities of the liquid electrolyte-soaked nanofiber separators. From Fig. 20 it is seen that at all temperatures, the ionic

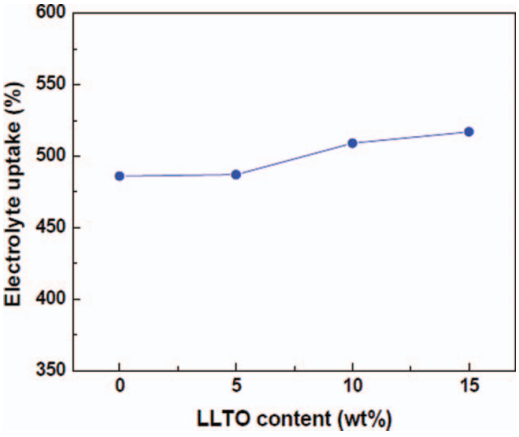

Figure 19. Electrolyte uptakes of electrospun LLTO/PAN nanofiber separators. The liquid electrolyte used was 1 M lithium hexafluorophosphate ($LiPF_6$) in 1:1 (V/V) ethylene carbonate/ethyl methyl carbonate. The electrolyte uptake increases slightly with increase in LLTO content (Color figure available online).

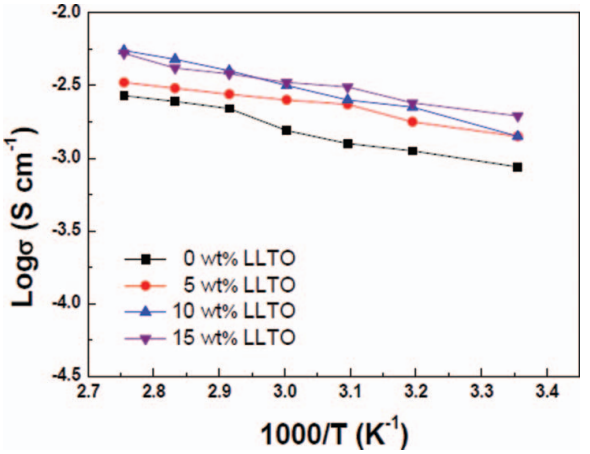

Figure 20. Ionic conductivities of liquid electrolyte-soaked electrospun LLTO/PAN nanofiber separators with different LLTO contents. The presence of LLTO particles decreases the fiber diameter and increases the surface area of LLTO/PAN nanofibers, which can help the nanofiber separators entrap more liquid electrolyte, i.e., leading to increased electrolyte uptake. This may be the main reason for the increased conductivities at high LLTO contents. In addition, LLTO has high bulk conductivity (10^{-3} S/cm at room temperature), which may also partially contribute to the enhanced conductivities of liquid electrolyte-soaked LLTO/PAN nanofiber separators. (Color figure available online).

conductivities increase with increase in LLTO content. The presence of LLTO particles decreases the fiber diameter and increases the surface area of LLTO/PAN nanofibers, which can help the nanofiber separators entrap more liquid electrolyte, i.e., leading to increased electrolyte uptake (Fig. 19). This may be the main reason for the increased conductivities at high LLTO contents. In addition, LLTO has high bulk conductivity (10^{-3} S/cm at room temperature).[78] Therefore, the high conductivity of LLTO may also partially contribute to the enhanced conductivities of liquid electrolyte-soaked LLTO/PAN nanofiber separators.

In addition to the ionic conductivities of liquid electrolyte-soaked nanofiber separators, the resistances at the interfaces of electrolyte-soaked separators and lithium electrodes are also important. The electrochemical impedance spectra of lithium/liquid electrolyte-soaked separator/lithium cells are shown in Fig. 21. The diameter of the intermediate-frequency semicircle indicates the electrode-electrolyte interfacial resistance R_i.[13] As shown in Fig. 21, the order of R_i values is: 15 wt% LLTO/PAN nanofiber separator <12 wt% LLTO/PAN nanofiber separator <10 wt% LLTO/PAN nanofiber separator <5 wt% LLTO/PAN nanofiber separator <0 wt% LLTO/PAN nanofiber separator. The addition of LLTO particles can help trap impurities from the liquid electrolyte, which may lead to smaller interfacial resistance at high LLTO contents.

In order to further examine the performance of using LLTO/PAN nanofiber separators in rechargeable lithium-ion batteries, electrochemical cells were fabricated with $LiFePO_4$ as the cathode and lithium metal as the counter electrode. The LLTO content in these nanofiber separators was 10 wt%. For comparison, the cells using commercial Celgard 2400 separator and pure PAN nanofiber separator were also prepared. The first-cycle charge and discharge curves at room temperature are shown in Fig. 22. All the curves show stable charge and discharge platforms, and the initial specific discharge capacities of all cells are between 148–162 mAh g^{-1}. However, cells using liquid electrolyte-soaked PAN nanofiber separator

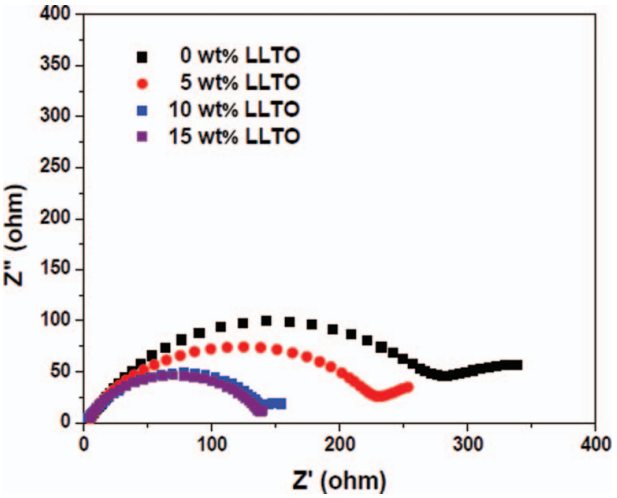

Figure 21. Electrochemical impedance spectra of liquid electrolyte-soaked LLTO/PAN nanofiber separators with different LLTO contents. The addition of LLTO particles can help trap impurities from the liquid electrolyte and lead to smaller interfacial resistance at high LLTO contents (Color figure available online).

have higher charge and discharge capacities than those using electrolyte-soaked Celgard 2400. Furthermore, the addition of LLTO particles in the PAN nanofiber separator further increases the capacities.

Figure 23 shows the cycling performance of cells containing different separators. At the 50th cycle, cells using liquid electrolyte-soaked LLTO/PAN nanofiber separator have

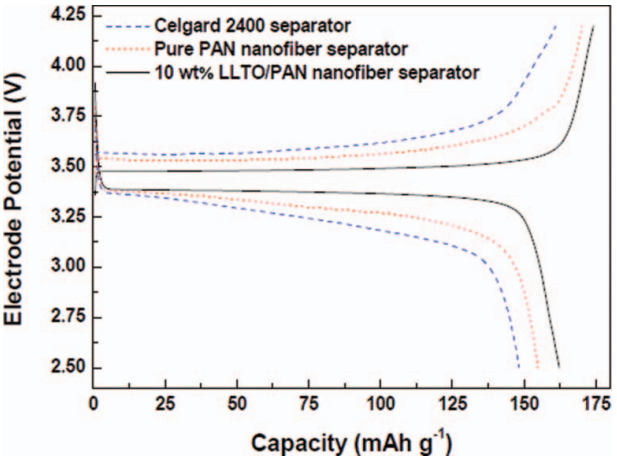

Figure 22. Charge-discharge curves of Li/$LiFePO_4$ cells using Celgard 2400 separator, pure PAN nanofiber separator, and LLTO/PAN nanofiber separator. Cells using liquid electrolyte-soaked PAN and LLTO/PAN nanofiber separators have higher charge and discharge capacities than those using electrolyte-soaked Celgard 2400 (Color figure available online).

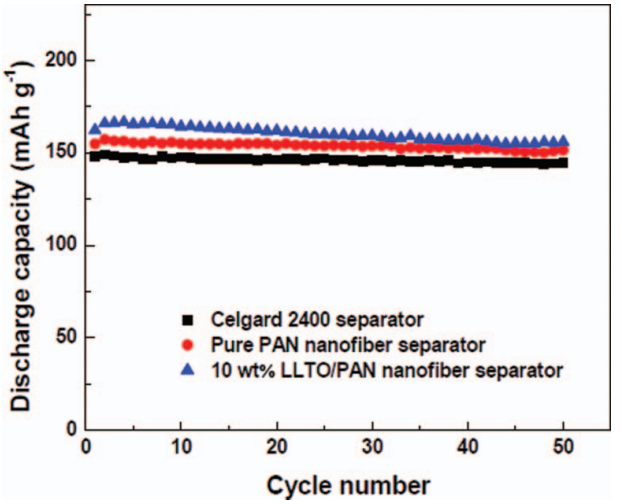

Figure 23. Cycle performance of Li/$LiFePO_4$ cells using Celgard 2400 separator, PAN nanofiber separator, and LLTO/PAN nanofiber separator. At the 50th cycle, cells using liquid electrolyte-soaked LLTO/PAN nanofiber separator have the highest discharge capacity of 156 mAh g^{-1}, which is 91.7% of the theoretical capacity (170 mAh g^{-1}) of $LiFePO_4$ (Color figure available online).

the highest discharge capacity of 156 mAh g^{-1}, which is 91.7% of the theoretical capacity (170 mAh g^{-1}) of $LiFePO_4$. That result confirms the excellent efficiency of the liquid electrolyte-soaked LLTO/PAN nanofiber separators to conduct lithium ions between electrodes during cycling. Therefore, LLTO/PAN nanofiber membranes are a promising separator candidate for rechargeable lithium-ion batteries.

6. Conclusions

Electrospun nanofibers are attractive as electrode materials since they have shorter diffusion path relative to the commonly employed powder materials and faster intercalation kinetics is expected due to their high area/mass ratio. Electrospun nanofibers also offer a relatively large number of lithium insertion sites, and therefore the charge-transfer resistance at the interface between the electrolyte and active electrode materials is decreased. Hence, electrospun nanofibers are advantageous for use as electrode materials in lithium-ion battery applications. In the case of electrospun nanofiber separators, they enable high-rate charge/discharge of batteries because of their high porosity and desirable pathways for ion transport.

In this review, novel Si/C nanofiber anodes, $LiFPO_4$/C nanofiber cathodes and LLTO-PAN nanofiber separators are discussed. For Si/C nanofiber anodes, the high volume change of Si nanoparticles during lithium insertion/extraction can be accommodated by encapsulating them into carbon nanofibers. Hence, the excellent electronic conductivity of carbon and the super-high Li storage of Si nanoparticle provide these composite nanofiber anodes with high capacity and good cycling stability. For $LiFePO_4$/C nanofiber cathodes, homogeneously-dispersed carbonaceous layer on $LiFePO_4$ and decreased particle size can be achieved by electrospinning and subsequent heat-treatment, and they lead to good cathode performance, such as satisfactory capacity and good cycling stability. In the case of

LLTO/PAN nanofiber separators, the liquid electrolyte-soaked nanofiber separators exhibit high electrolyte uptake, low interfacial resistance, and good compatibility with lithium electrode, and cells using these nanofiber separators have high capacity and stable cycle performance. These results demonstrate that electrospinning is a promising approach to prepare high-performance nanofiber anodes, nanofiber cathodes, and nanofiber separators that can replace current commercially-used materials for lithium-ion batteries.

The major challenges of using electrospinning nanofibers in lithium-ion batteries are the relatively low production rate and high cost of the electrospinning process. In addition, the processing-structure-performance relationship of these novel electrospun battery materials is not well-understood. Currently, the industry is developing and commercializing production-scale electrospinning machines that can potentially produce electrospun nanofibers at high rates and with low cost. Work in our laboratory and other groups is also in progress aimed at studying both the relationship between the process, structure, and performance of these novel electrospun nanofiber-based battery materials, and the structure and performance improvement of nanofiber anodes, nanofiber cathodes, and nanofiber separators.

Acknowledgments

This work was supported by the US Department of Energy (DE-EE0001177), the ERC Program of the National Science Foundation Award (No. EEC-08212121) and the National Textile Center/U.S. Department of Commerce (IT09IAX113001).

References

1. Padbury, R.; Zhang, X. "Lithium-oxygen batteries - limiting factors that affect performance," *J. Power Sources*, **2011**, *196*, 4436–4444.
2. Tarascon, M.; Armand, M. "Issues and challenges facing rechargeable lithium batteries," *Nature*, **2001**, *414*, 359–367.
3. Long, J. W.; Dunn, B.; Rolison, D. R.; White, H. S. "Three-dimentsional battery architectures," *Chem. Rev.*, **2004**, *104*, 4463–4492.
4. Ji, L.; Zhang, X. "Ultrafine polyacrylonitrile/silica composite nanofibers via electrospinning," *Mater. Lett.*, **2008**, *62*, 2165–2168.
5. Guo, Y. G.; JHu, J. S.; Wan, L. J. "Nanostructured materials for electrochemical energy conversion storage devices," *Adv. Mater.*, **2008**, *20*, 2878–2887.
6. Manthiram, A.; Vadivel Murugan, A.; Sarkar, A.; Muraliganth, T. "Nanostructured electrode materials for electrochemical energy storage and conversion," *Energy Environ. Sci.*, **2008**, *1*, 621–638.
7. Saunier, J.; Alloin, F.; Sanchez, J. Y.; Caillon, G. "Thin and flexible lithium-ion batteries: Investigation of polymer electrolytes," *J. Power Sources*, **2003**, *119*, 454–459.
8. Lee, Y.M.; K. J. W.; Choi, N. S.; Lee, J.A.; Seol, W.H.; Park, J.K. "Novel porous separator based on PVdF and PE non-woven matrix for rechargeable lithium batteries," *J. Power Sources*, **2005**, *139*, 235–241.
9. Ooms, F. G. B. "Performance of Solupor (R) separator materials in lithium ion batteries," *J. Power Sources*, **2001**, *97–98*, 598–601.
10. Cho, T.-H. "Battery performances and thermal stability of polyacrylonj. power sourcesitrile nano-fiber-based nonwoven separators for li-ion battery," *J. Power Sources*, **2008**, *181*, 155–160.
11. Arora, P. K.; Zhang, Z. M. "Battery separators," *Chem. Rev.*, **2004**, *104*, 4419–4462.
12. Zhang, S. S. "A review on the separators of liquid electrolyte li-ion batteries," *J. Power Sources*, **2007**, *164*, 351–364.

13. Jung, H. R.; Ju, D. H.; Lee, W. J.; Zhang, X. W.; Kotek, R. "Electrospun hydrophilic fumed silica/polyacrylonitrile banofiber-based composite electrolyte membranes," *Electrochimica Acta*, **2009**, *54*, 3630–3637.
14. Yang, C. R.; Jia, Z. D.; Guan, Z. C.; Wang, L. M. "Polyvinylidene fluoride membrane by novel electrospinning system for separator of li-ion batteries," *J. Power Sources*, **2009**, *189*, 716–720.
15. Bansal, D.; Meyer, B.; Salomon, M. "Gelled membranes for li and li-ion batteries prepared by electrospinning," *J. Power Sources*, **2008**, *178*, 848–851.
16. McCann, J. T.; Li, D.; Xia, Y. "Electrospinning of nanofibers with core-sheath, hollow, or porous structures," *J. Mater. Chem.*, **2005**, *15*, 735–738.
17. Norris, I. D.; Shaker, M. M.; Ko, F. K.; MacDiarmid, A. G. "Electrostatic fabrication of ultrafine conducting fibers: Polyaniline/polyethylene oxide blends," *Synth. Met.*, **2004**, *114*, 109–114.
18. Li, D.; Xia, Y. "Electrospinning of nanofibers: Reinventing the wheel," *Adv. Mater.*, **2004**, *16*, 1151–1170.
19. Norris, I. D.; Shaker, M. M.; Ko, F. K.; MacDiarmid, A. G. "Electrostatic fabrication of ultrafine conducting fibers: Polyaniline/polyethylene oxide blends," *Synth. Met.*, **2004**, *114*, 109–114.
20. Gibson, P.; Schreuder-Gibson, H.; Rivin, D. "Transport properties of porous membranes based on electrospun nanofibers," *Colloid and Surfaces A: Physicochem. Engr. Aspects*, **2001**, *469*, 187–188.
21. Park, S. H.; Kim, C.; Choi, Y. O.; Yang, K. S. "Preparation of pitch-based CF/ACF webs by electrospinning," *Carbon*, **2003**, *41*, 2655–2657.
22. Wang, Y.; Serrano, S.; Santiago-Aviles, J. J. "Raman characterization of carbon nanofibers prepared using electrospinning," *Synth. Met.*, **2003**, *138*, 423–427.
23. Yang, K. S.; Edie, D. D.; Lim, D. Y.; Kim, Y. M.; Choi, Y. O. "Preparation of carbon fiber web from electrostatic spinning of PMDA-ODA poly(amic acid) solution," *Carbon*, **2003**, *41*, 2039–2046.
24. Kim, C.; Yang, K. S. "Electrochemical properties of carbon nanofiber web as an electrode for supercapacitor prepared by electrospinning," *Appl. Phys. Lett.*, **2003**, *83*, 1216–1218.
25. Dai, H.; Gong, J.; Kim, H.; Lee, D. "A novel method for preparing ultra-fine alumina-borate oxide fibres via an electrospinning technique," *Nanotechnology*, **2002**, *13*, 674–677.
26. Sigmund, W. "Processing and structure relationships in electrospinning of ceramic fiber systems," *J. Am. Ceram. Soc.*, **2006**, *89*, 395–407.
27. Zhang, G. "Electrospun nanofibers for potential space-based applications," *Mat. Sci. Eng. B-Solid*, **2005**, *116*, 353–358.
28. Choi, S. S.; Lee, S. G.; Im, S. S.; Kim, S. H.; Joo, Y. L. "Silica nanofibers from electrospinning/sol-gel process," *J. Mater. Sci. Lett.*, **2003**, *22*, 891–893.
29. Larsen, G.; Velarde-Ortiz, R.; Minchow, K.; Barrero, A.; Losertales, I. G. "A method for making inorganic and hybrid (organic/inorganic) fibers and vesicles with diameters in the submicrometer and micrometer range via sol-gel chemistry and electrically forced liquid jets," *J. Am. Chem. Soc.*, **2003**, *125*, 1154–1155.
30. Yuh, J.; Nino, J. C.; Sigmund, W. "Synthesis of barium titanate ($BatiO_3$) nanofibers via electrospinning," *Mater. Lett.*, **2005**, *59*, 3645–3647.
31. Wang, M.; Singh, H.; Hatton, T. A.; Rutledge, G. C. "Field-responsive superparamagnetic compsoite nanofibers by electrospinning," *Polymer*, **2004**, *45*, 5505–5514.
32. Viswanthamurthi, P. "GeO_2 fibers: Preparation, morphology and photoluminescence property," *J. Ceram. Phys.*, **2004**, *121*, 441–445.
33. Madhugiri, S.; Sun, B.; Smirniotis, P. G.; J.P., F.; Balkus, K. J. "Electrospun mesoporous titanium dioxide fibers," *Micropor. Mesopor. Mater.*, **2004**, *69*, 77–83.
34. Shao, C. L.; Guan, H. Y.; Liu, Y. C.; Yu, R.; Yang, X. H. "A novel method for making ZrO_2 nanofibers via an electrospinning technique," *J. Cryst. Growth.*, **2004**, *267*, 380–384.
35. Jing, N.; Wang, M.; Kameoka, J. "Fabrication of ultrathin ZrO_2 nanofiber by electrospinning," *J. Photopolym. Sci. Tech.*, **2005**, *18*, 503–506.
36. Ji, L.; Zhang, X. "Fabrication of porous carbon/si composite nanofibers as high-capacity battery electrodes," *Electrochem. Commun.*, **2009**, *11*, 1146–1149.

37. Ji, L.; Jung, K. H.; Medford, A. J.; Zhang, X. "Electrospun polyacrylontrile nanofibers with embedded si nanoparticles and their electrochemical behaviors after carbonization," *J. Mater. Chem.*, **2009**, *19*, 4992–4997.
38. Ji, L.; Zhang, X. "Electrospun carbon nanofibers containing silicon particles as an energy storage medium," *Carbon*, **2009**, *47*, 3219–3226.
39. Fan, X.; Zou, L.; Zheng, Y. P.; Kang, F. Y.; Shen, W. C. "Electrospinning preparation of nanosilicon/disordered carbon composite as anode materials in li-ion battery," *Electrochem. Solid State Lett.*, **2009**, *12*, A199–A201.
40. Ji, L.; Lin, Z.; Medford, A. J.; Zhang, X. "In-situ encapsulation of nickel particles in electrospun carbon nano-fibers and their electrochemical performance," *Chem. A Eur. J.*, **2009**, *15*, 10718–10722.
41. Ji, L., Lin, Z., Zhang, X. "Formation and electrochemical performance of copper/carbon composite nanofibers," *Electrochim ACTA*, **2010**, *55*, 1605–1611.
42. Wang, L.; Yu, Y.; Chen, P. C.; Zhang, D. W.; Chen, C. H. "Electrospinning synthesis of C/Fe3O4 composite nanofibers and their application for high performance lithium-ion batteries," *J. Power Sources*, **2008**, *183*, 717–723.
43. Wang, L.; Yu, Y.; Chen, P. C.; Chen, C. H. "Electrospun carbon-cobalt composite nanofibers as an anode material for lithium ion batteries," *Scripta Materialia*, **2008**, *58*, 405–408.
44. Yu, Y.; Gu, L.; Zhu, C. B.; van Aken, P. A.; Maier, J. "Tin nanoparticles encapsulated in porous multichannel carbon microtubes: Preparation by single-nozzle electrospinning and application as anode material for high-performance li-based batteries," *J. Am. Chem. Soc.*, **2009**, *131*, 15984–15985.
45. Yu, Y. "Encapsulation of sn@carbon nanoparticles in bamboo-like hollow carbon nanofibers as an anode material in lithium-based batteries," *Angew. Chem.-Int. Ed.*, **2009**, *48*, 6485–6489.
46. Zou, L. "Sn/C non-woven film prepared by electrospinning as anode materials for lithium ion batteries," *J. Power Sources*, **2010**, *195*, 1216–1220.
47. Ji, L.; Zhang, X. "Manganese oxide nanoparticle-loaded porous carbon nanofibers as anode materials for high-performance lithium-ion batteries," *Electrochem. Commun.*, **2009**, *11*, 795–798.
48. Ji, L.; Medford, A. J.; Zhang, X. "Porous carbon nanofibers loaded with manganese oxide particles: Formation mechanism and electrochemical performance as energy storage materials," *J. Mater. Chem.*, **2009**, *19*, 5593–5601.
49. Ji, L.; Lin, Z.; Medford, A. J.; Zhang, X. "Porous carbon nanofibers from electrospun polyacrylonitrile/SiO_2 composites as an energy storage material," *Carbon*, **2009**, *47*, 3346–3354.
50. Ji, L.; Zhang, X. "Generation of activated carbon nanofibers from electrospun polyacrylonitrile-zinc chloride composites for use as anodes in lithium-ion batteries," *Electrochem. Commun.*, **2009**, *11*, 684–687.
51. Ji, L.; Zhang, X. "Fabrication of porous carbon nanofibers and their application as anode materials for rechargeable lithium-ion batteries," *Nanotechnol.*, **2009**, *20*, 155705 (7 pp.).
52. Kasavajjula, U.; Wang, C.; Appleby, A. J. "Nano-and bulk-si-based insertion anodes for lithium-ion secondary cells," *J. Power Sources*, **2007**, *163*, 1003–1039.
53. Lin, Z.; Ji, L.; Woodroof M.D.; Zhang, X. "Electrodeposited mnox/carbon nanofiber composites for use as anode materials in rechargeable lithium-ion batteries," *J. Power Sources*, **2010**, *195*, 5025–5031.
54. Ji, L.; Zhang, X. "Fabrication of carbon nanofiber-driven electrodes from electrospun polyacrylonitrile/polypyrrole bicomponents for high-performance rechargeable lithium-ion batteries," *J. Power Sources*, **2010**, *195*, 2050–2056.
55. Kim, C. "Raman spectroscopic evaluation of polyacrylonitrile-based carbon nanofibers prepared by electrospinning," *J. Raman Spectroscopy*, **2004**, *35*, 928–933.
56. Zussman, E. "Mechanical and structural characterization of electrospun PAN-derived carbon nanofibers," *Carbon*, **2005**, *43*, 2175–2185.
57. Babu, V. S.; Seehra, M. S. "Modeling of disorder and X-ray diffraction in coal-based graphitic carbons," *Carbon*, **1996**, *34*, 1259–1265.

58. Chan, C. K. "High performance lithium battery anodes using silicon nanowires," *Nat. Nanotechnol.*, **2008**, *3*, 31–35.
59. Cui, L. F.; Ruffo, R.; Chan, C. K.; Peng, H. L.; Cui, Y. "Crystalline-amorphous core−shell silicon nanowires for high capacity and high current battery electrodes," *Nano Lett.*, **2009**, *9*, 491–495.
60. Wilson, A. M.; Dahn, J. R. "Lithium insertion in carbons containing nanodispersed silicon," *J. Electrochem. Soc.*, **1995**, *142*, 326–332.
61. Reindl, S.; Aldabergenova, E.; Frank, A. G.; Peukert, W. "Dispersing silicon nanoparticles in a stirred media mill-investigating the evolution of morphology, structure and oxide formation," *Phys. Stat. Sol.*, **2007**, *204*, 2329–2338.
62. Hu, Y. S. "Superior storage performance of a Si@SiOx/c nanocomposite as anode material for lithium-ion batteries," *Angew Chem. Int. Ed.*, **2008**, *47*, 1645–1649.
63. Gu, Y. X.; Chen, D. R.; Jiao, M. L. "Synthesis and electrochemical properties of nanostructured LiCoO2 fibers as cathode materials for lithium-ion batteries," *J. Phys. Chem. B.*, **2005**, *109*, 17901–17906.
64. Toprakci, O.; Ji, L.; Lin, Z.; Toprakci, H. A. K.; Zhang, X. "Fabrication and electrochemical characteristics of electrospun LiFePO4/carbon composite fibers for lithium-ion batteries," *J. Power Sources*, **2011**, 1016.
65. Shao, C. L.; Yu, N.; Liu, Y. C.; Mu, R. X. "Preparation of LiCoO2 nanofibers by electrospinning technique," *J. Phys. Chem. Solids*, **2006**, *67*, 1423–1426.
66. Gu, Y. X.; Chen, D. R.; Jiao, X. L.; Liu, F. F. "LiCoO2-MgO coaxial fibers: Co-electrospun fabrication, characterization and electrochemical properties," *J. Mater. Chem.*, **2007**, *17*, 1769–1776.
67. Lu, H. W.; Yu, L.; Zeng, W.; Li, Y. S.; Fu, Z. W. "Fabrication and electrochemical properties of three-dimensional structure of LiCoO2 fibers," *Electrochem. Solid State Lett.*, **2008**, *11*, A140–A144.
68. Ding, Y. H.; Zhang, P.; Long, Z. L.; Jiang, Y.; Xu, F. "Synthesis and electrochemical properties of LiNi1/3Co1/3Mn1/3O2 and LiNi3/8Co1/4Mn3/8O2 nanofibers," *Rare Metal Mater. Engr.*, **2009**, *38*, 1227–1229.
69. Ding, Y. H.; Zhang, P.; Long, Z. L.; Jiang, Y.; Xu, F. "Morphology and electrochemical properties of al doped LiNi1/3Co1/3Mn1/3O2 nanofibers prepared by electrospinning," *J. ALLOYS Compd.*, **2009**, *487*, 507–510.
70. Padhi, A. K.; Nanjundaswamy, K. S.; Masquelier, C.; Okada, S.; Goodenough, J. B. "Effect of structure on the Fe3+/Fe2+ redox couple in iron phosphates," *J. Electrochem. Soc.*, **1997**, *144*, 1609–1613.
71. Chung, S. Y.; Bloking, J. T.; Chiang, Y. M. "Electronically conductive phospho-olivines as lithium storage electrodes," *Nature Materials*, **2002**, *1*, 123–128.
72. Dalton, S.; Heatley, F.; Budd, P. M. "Thermal stabilization of polyacrylonitrile fibres," *Polymer*, **1999**, *40*, 5531–5543.
73. Streltsov, V. A.; Belokoneva, E. L.; Tsirelson, V. G.; Hansen, N. K. "Multipole analysis of the electron density in triphylite, LiFePO4, using X-ray diffraction data," *Acta Cryst.*, **1993**, *B49*, 147–153.
74. Gao, K.; Hu, X. G.; Dai, C. S.; Yi, T. F. "Crystal structures of electrospun PVDF membranes and its separator application for rechargeable lithium metal cells," *Mater. Sci. Engr. B-Solid State Mater. Adv. Technol.*, **2006**, *131*, 100–105.
75. Liang, Y.; Zhang, X. "Preparation and electrochemical characterization of ionic-conducting lithium lanthanum titanate oxide/polyacrylonitrile submicron composite fiber-based lithium-ion battery separators," *J. Power Sources*, **2010**, *196*, 436–441.
76. Cho, T. H. "Electrochemical performances of polyacrylonitrile nanofiber-based nonwoven separator for lithium-ion battery," *Electrochem. Solid State Lett.*, **2007**, *10*, A159–A162.
77. Choi, S. W.; Kim, J. R.; Jo, S. M.; Lee, W. S.; Kim, Y. R. "Electrochemical and spectroscopic properties of electrospun PAN-based fibrous polymer electrolytes," *J. Electrochem. Soc.*, **2005**, *152*, A989–A995.
78. Stramare, S.; Thangadurai, V.; Weppner, W. "Lithium lanthanum titanates: A review," *Chem. Mater.*, **2003**, *15*, 3974–3990.